Journal of Inorganic and Organometallic Polymers and Materials (2020) 30:4382–4393
https://doi.org/10.1007/s10904-020-01669-5

Preparation and Properties of Silver-Based Cellulose/Polyvinyl Alcohol Antibacterial Materials

Zhaoqi Wang[1] · Shengli Zhao[1] · Ling Hong[1] · Jintian Huang[1]

Received: 11 March 2020 / Accepted: 12 July 2020 / Published online: 2 September 2020

Abstract
This paper reports the synthesis and application of nanosilver antibacterial materials. The preparation methods of nanosilver complexes are described. The effect of silver nitrate concentration and nanosilver dispersion on antibacterial properties was analysed. In this experiment, TEMPO oxidant was used to oxidize hydroxyl on the C_6 position of wood nanocellulose into a carboxyl group. Meanwhile, carboxyl compound was used to react with $AgNO_3$, the silver composite material was prepared with PVA as the substrate. We use interface grafting. The surface of cellulose is bonded with reactive functional groups to form a transition layer. To improve the interface bonding between matrix and reinforcing fiber. The Ag-NC-PVA nanocomposite film was characterized by UV–Vis, SEM, TEM, mechanical properties and antibacterial properties analysis. SEM and TEM images showed that the size of most silver nanoparticles ranged from 5 to 20 nm; the mean particle size was 10 nm. The mechanical properties of Ag-NC-PVA films were greater than that of PVA film. When the amount of Ag-NC was 4%, its tensile strength was 71.3 MPa; it's almost 15% higher than PVA. After antibacterial analysis, Ag-NC endowed PVA with excellent antibacterial properties. The prepared Ag-NC-PVA greatly promotes the practical application development of the silver-based composite bacteriostatic material.

Keywords Nanosilver · Interface bonding · Nanocellulose · Mechanical properties · Antibacterial materials

1 Introduction

In recent years, with the continuous development of nanotechnology in the field of materials, many new materials have emerged, such as: nanomaterials. Then came a new era of nanomaterials. Nanosilver was an advanced functional material; nanosilver had the characteristics of small size effect, surface effect and macroscopic quantum tunnelling effect. It had an important application value in optoelectronics, biosensing, catalysis, antibacterial, etc. It can be applied to optical materials [1–4], catalyst materials [5–8], antibacterial materials [9–15], biosensor materials [16, 17], battery electrode materials [18–20], low temperature superconductor materials [21], etc. Silver nanoparticles (AgNPs) have been widely used due to its broad spectrum of antimicrobial activities and low toxicity toward mammalian cells [22, 23].

At present, there were many ways to prepare nanosilver. According to the principle of preparation, the preparation methods of silver nanoparticles can be divided into three categories: Physical method [24, 25]. Chemical method [26, 27]. Biological method [28, 29]. Among them, the physical method was widely used, the operation process was simple and produced fewer impurities, but the product was easy to reunite, the required equipment requires high technology, expensive production costs, and unable to mass production. The second, biological method for preparing nanosilver only stays in the research stage. Due to the low purity of microorganisms and the general biological reducibility was weak, one of the reasons why it cannot be applied on a large scale. Also, most chemical synthesis of silver nanoparticles was to reduce Ag^+, thereby obtaining a silver atom, and form elemental silver particles, the advantage of this method was that many of metal nanoparticles could be produced in a short time. Moreover, the pore diameter and size distribution of metal nanoparticles can be better controlled. However, the nanosilver produced by this faster method. Nanoparticles have high surface energy; they were very easy to reunite [30]. Therefore, some amounts of dispersant or stabilizer

✉ Jintian Huang
jintian_h@163.com

[1] College of Material Science and Art Design, Inner Mongolia Agricultural University, Hohhot, China

were needed, such as: PVP(polyvinyl alcohol)to control the process of reaction. But this process cost was high, pollute the environment, need to improve urgently. Antibacterial mechanism of nanosilver [31]: silver ion contact reaction, causes the microorganism common component destruction or produces the function barrier. When tiny amounts of silver ions reach the membrane of a microbial cell, because the latter was negatively charged, rely on coulomb gravity to make the two firmly adsorb, the silver ions penetrate the cell wall and enter the cell, and reacts with the oxygen metabolism enzyme -SH group, coagulate the protein, the activity of cell synthase was destroyed. Cellulose the ability to divide and multiply and die. Silver ions can also destroy microbial electron transport systems, respiratory systems and material transport systems.

The interface of composite materials is not a simple geometric plane. It is a three-dimensional interfacial phase [32, 33] containing the transition region between the two phases. The chemical composition, molecular arrangement, thermal properties and mechanical properties of the interfacial phase show a continuous gradient change. The interface phase is very thin and submicroscopic, but it has an extremely complex structure. Thermal stress [34, 35], interfacial chemical effect [36] and the interfacial crystallisation [37–39] can occur in the composite process of PVA and silver-bearing cellulose. The interface microstructure and properties caused by these effects have a direct impact on the macroscopic properties of composites. In this experiment, a unique method was adopted: the composite antibacterial material was prepared by using nanocellulose as dispersion, silver-carrying nanocellulose as filler, and polyvinyl alcohol [40, 41] as substrate. Its cost reduction, resource-saving and mechanical performance [42] have been significantly improved. This nanosilver PVA material [43], which was dispersed by nanocellulose, can be made into dry material, according to demand can also be prepared as a gel material. It is widely used in food packaging, chemical catalysis [44], environmental protection and other fields,it has a good development prospect.

2 Materials and Methods

2.1 Materials

The pulp board (obtained from Hohhot, Inner Mongolia, China). Polyvinyl alcohol and sodium hypochlorite purchased from Fuchen (Tianjin) Chemical Reagent Co. Ltd, China. Silver nitrate was purchased from Tianjin Tiangan Chemical Technology Development Co. Ltd, China. Sodium bromide and sodium borohydride were purchased from Tianjin Shengao Chemical Reagent Co. Ltd, China. Other reagents applied in this experiment were analytical grade (Scheme 1).

2.2 Extraction of Nanocellulose

2.2.1 Pretreatment of Cellulose

To remove lignin and hemicelluloses from the pulp, the fiber needs to be pretreated. The pulp board (obtained from Hohhot, Inner Mongolia, China) was torn, sealed and stored for later use. A certain amount of samples were weighed and put into a conical flask with deionised water (DW) at

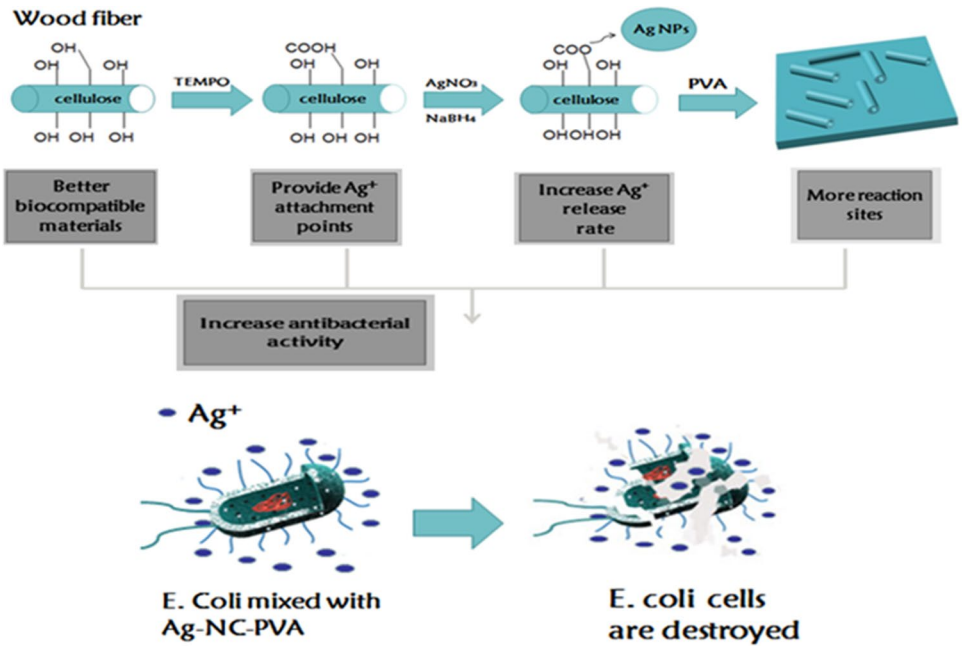

Scheme 1 Schematic diagram of preparation of silver-based cellulose/PVA antibacterial materials

75 °C. Then, $HClO_2$ and CH_3COOH were separately added and repeated five times. After pretreatment, cellulose was filtered repeatedly by multi-purpose vacuum pump of deionised water and dried at room temperature for a night.

2.2.2 Preparation of Nanocellulose

Nanocellulose is obtained by NaOH/urea/thiourea aqueous solvent system. The pretreated cellulose was added to the NaOH/urea/thiourea aqueous solvent system. Under the condition of ice salt bath, the mixture was stirred for 2 h to fully dissolve cellulose. Finally, the uniformly dispersed nanocellulose could be obtained by ultrasonic treatment for 1 h.

2.2.3 Preparation of Oxidized Nanocellulose

To obtain oxidized nanocellulose, Weigh the quantitative Na_2CO_3 and $NaHCO_3$ as buffer solutions, the ratio of Na_2CO_3 and $NaHCO_3$ was 7:3, the total concentration was 0.1 mol/L. Then weigh 0.5 g TEMPO and 1 g NaBr in turn, and dissolve it in the configured buffer solution; secondly, 2.5 g nanocellulose was dispersed in the above solvent, weigh the quantitative NAClO solution separately, during the mixing process, slowly add a dilute hydrochloric acid solution to adjust the pH between 10 and 11. Finally, the adjusted pH of NaClO solution was slowly added drop wise to the wood cellulose suspension. Keep stirring for reaction, after 4 h reaction, wash with deionised liquid until neutral, different carboxyl content of oxidized cellulose was obtained; the obtained oxidized cellulose was further formulated into different volumes of water dispersion system. Water dispersion system of nanocellulose with different carboxyl content was obtained by ultrasonic treatment.

2.3 Synthesis of Silver Nanoparticles (AgNPs)

Adding quantitative silver nitrate to nanocellulose aqueous dispersions with different carboxyl contents, the carboxyl group was fully complexed with Ag^+. And then the COOH-Ag^+ system, adding quantitative $NaBH_4$ (as a reducing agent) reduction of Ag^+ complexed by carboxyl groups, the resulting silver-loaded nanocellulose (Ag-NC) solution with different degrees of dispersion. By this method, silver nanoparticles were prepared and successfully grown on the nanocellulose. The resultant suspension was stored before further treatment.

2.4 Preparation of PVA, Ag-NC and Ag-NC-PVA Nanocomposite Films

Add 10 g of polyvinyl alcohol to 100 mL of deionised water, after magnetic stirring in 90 °C water bath for 2 h form a homogeneous solution with a volume fraction of 10%. Take a certain volume of Ag-NC suspension, the volume fraction of nanosilver was 1 wt%, 3 wt%, 4 wt% and 5wt% respectively (relative to nanocellulose solution mass). The Ag-NC films were prepared with different loadings of AgNPs. Add to PVA solution; then magnetic stirring was performed for 2 h in 45 °C water bath, in the defoaming vacuum machine (vacuum degree is − 0.9Mpa), vacuum defoaming was done for 1 h at room temperature. Pour it into the dish, place in a drying oven at 60 °C to dry, then cure the release films, the composite films with different Ag-NC-PVA content were obtained. The volume fraction of Ag-NC-PVA was 1 wt%, 3 wt%, 4 wt% and 5 wt%. Recorded as, Ag-NC-1PVA, Ag-NC-3PVA, Ag-NC-4PVA, Ag-NC-5PVA.

2.5 Characterization Techniques

The structure of nanocellulose and oxidised nanocellulose composites were analysed by FTIR (Tensor 27, Bruker, Germany). Measurement conditions: Resolution is 0.5 cm^{-1}. The frequency range is 400 ~ 4000 cm^{-1}. 2 mg samples are evenly mixed with 200 mg pure KBr, and they are placed in a mould and pressed into the thin sheet at 8–10 MPa for 2 min. Particles diameter should be less than 2 µm. KBr is used as contrast. The morphology of the Ag-NC-PVA was analysed by transmission electron microscopy (TEM) using an FEI Tecnai G2 20 with an accelerating voltage of 200 kV. Thermal analysis of the Ag-NC-PVA sample was measured using an STA 409 PC. The temperature ranged from 25 to 600 °C with a heating rate of 10 °C min^{-1} under nitrogen. The surface morphology of the material was observed by scanning electron microscopy (SEM). The composite was taken under a 10 kV Hitachi S4800 microscope. Ultraviolet absorbance measurements were taken on a TU-1950 UV Dual-Beam Visible Spectrophotometer. The formation of silver nanoparticles in a colloidal solution of 200 ~ 800 nm was observed. The mechanical properties of PVA and Ag-NC-PVA composite film were measured using microcomputer controlled universal testing machine (5940 Instron, USA). The tensile strength and elongation at break of PVA and Ag-NC-PVA were measured. The tensile strength was measured according to GB/T 13022-91, the experimental speed is 20 mm/min. To ensure data accuracy and repeatability, at least five measurements were carried out for each composite film.

3 Results and Discussion

3.1 Fourier Transforms Infrared (FT-IR) Analysis

Fourier transform infrared spectroscopy is an important method to observe the chemical structure of materials. Figure 1 shows the FT-IR spectra of oxidized nanocellulose and

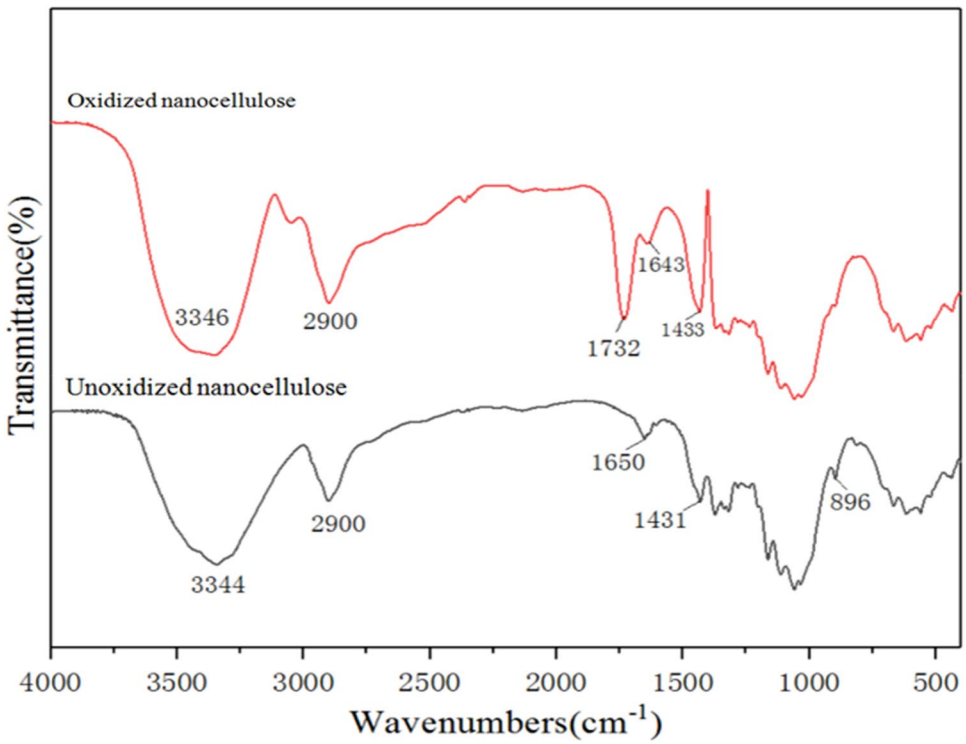

Fig. 1 Shows the FT-IR spectra of oxidized nanocellulose and unoxidized nanocellulose

unoxidized nanocellulose. For spectrum of nanocellulose, it shows the strong absorption at 3500 cm^{-1} ~ 3100 cm^{-1} ascribed to the stretching vibration peak of –OH in nanocellulose. With the addition of TEMPO, its characteristic peaks appeared. For spectrum of oxidized cellulose, the peak near 1732 cm^{-1} was the stretching vibration of C=O bonds at the carboxyl group. However, on the unoxidized nanocellulose, there is no stretching vibration peak. This indicates that the hydroxyl group of nanocellulose on C_6 has been successfully oxidized to carboxyl group. Besides, due to the unique structure of nanocellulose, there are some abnormal spectrum phenomena, which lead to baseline deviation of FTIR and weaken signal absorption of functional groups. But, it can also reveal that TEMPO modified the nanocellulose by oxidation and successfully prepared the nanocellulose.

3.2 UV–Vis Analysis

Figure 2 shows the UV absorption spectra of Ag-NC-PVA solutions at different concentrations. From top to bottom are Ag-NC-5PVA, Ag-NC-4PVA, Ag-NC-3PVA, Ag-NC-1PVA and PVA. Ultraviolet absorbance measurements were taken on a TU-1950 UV Dual-Beam Visible Spectrophotometer. The formation of silver nanoparticles in a colloidal solution of 200 ~ 800 nm was observed. Monitor color changes in colloidal solutions by visual inspection. Digital images of the sample were captured using a digital camera (cannon-550d) with a 4 × optical zoom. Figure 3 shows four different silver-containing cellulose-loaded polyvinyl alcohol colloidal solutions. Figure 3 was the ultraviolet absorption spectrum of silver-loaded polyvinyl cellulose colloidal solution with different silver content. We could see, except for the pure PVA solution, the remaining solution had a distinct characteristic peak at 200 nm–800 nm. The absorption peak wavelength of the largest characteristic peak was around 400 nm; the maximum characteristic absorption peak wavelengths were 403 nm and 398 nm respectively. This peak was a characteristic absorption peak of nanosilver ions; this was caused by the surface ion resonance of Ag nanoparticles. It shows that Ag^+ in silver nitrate solution was successfully reduced to Ag nanoparticles and adsorbed in the nanocellulose skeleton. The absorption light intensity of Ag-NC-PVA solution also increases with the increase of silver ion concentration. When the concentration of silver ions was maximum, its absorbance [45] was the maximum and transmittance the minimum,it shows that the concentration of silver ion was the biggest factor affecting the transmittance. Figure 2 was shown from left to right, Ag-NC-5PVA, Ag-NC-1PVA, Ag-NC-3PVA, Ag-NC-4PVA.

3.3 SEM Analysis

Figure 3 is the scanning electron microscopy of nanocellulose polyvinyl alcohol membrane with different silver content. As can be seen from the figure, the surface of pure PVA is relatively smooth. After carrying silver, bright spherical particles can be seen, and the distribution is uniform, without flocculent phenomenon. Through SEM–EDS analysis

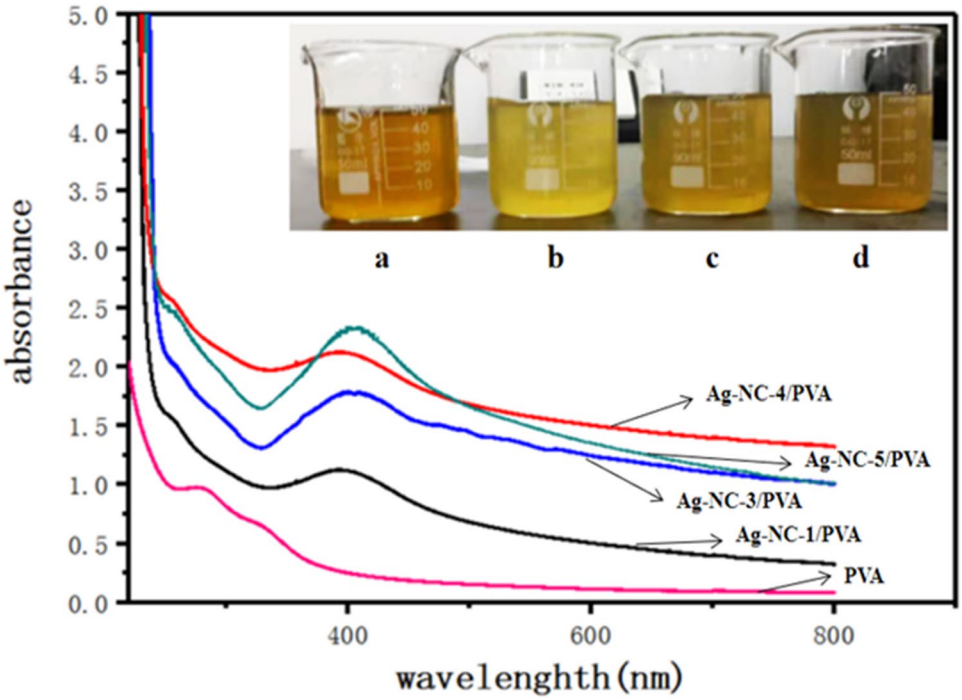

Fig. 2 Shows Ag-NC-PVA solution of different concentration and ultraviolet absorption spectrum of Ag-NC-PVA solution

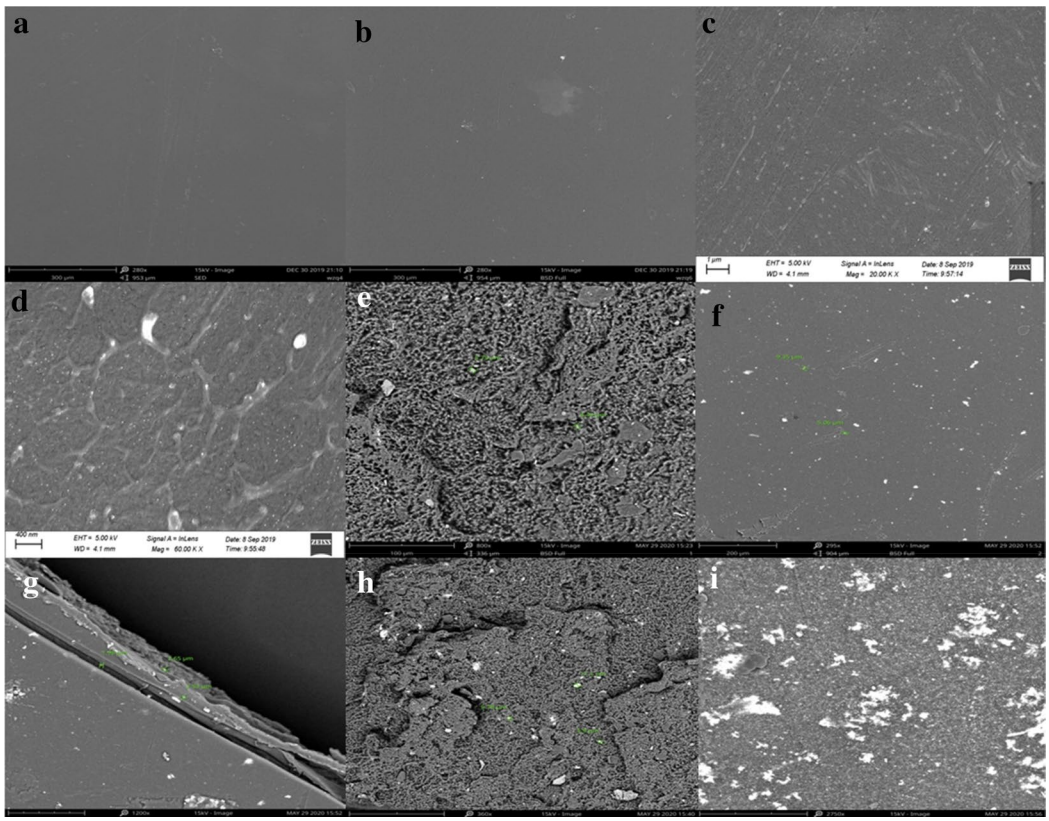

Fig. 3 SEM of nanocellulose polyvinyl alcohol membrane

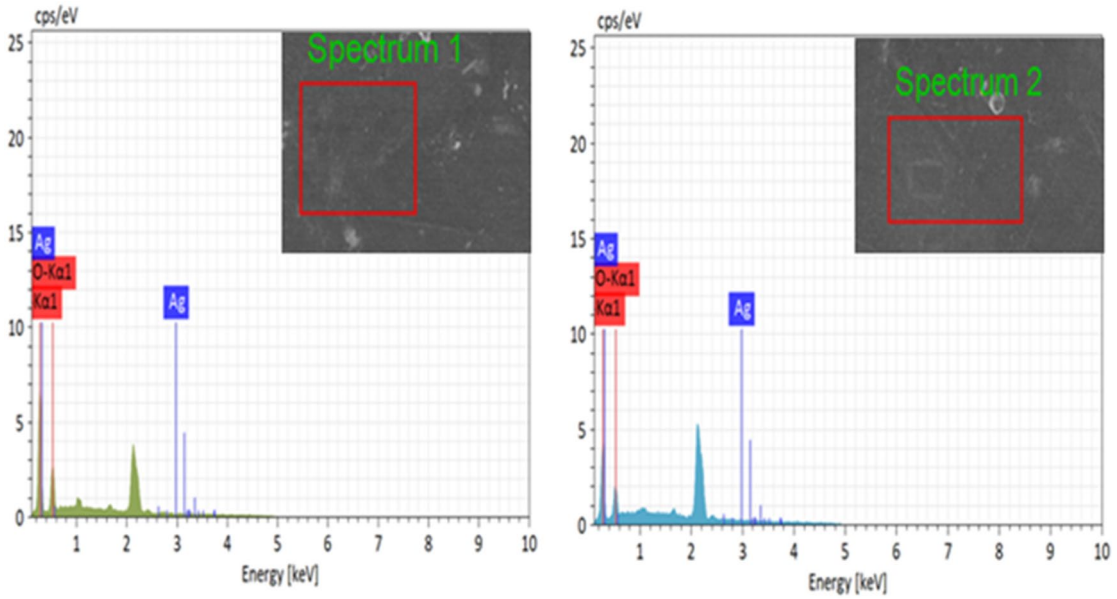

(a) Substrate before silver loading (b) Substrate after silver loading

Fig. 4 SEM–EDS spectra of the samples

in Fig. 4, it was confirmed that the spherical particles were indeed nanometer silver particles. With the addition of Ag-NC content, a large number of folds and dorsal ridges gradually appeared on the composite membrane surface. This may be the addition of too much nanocellulose to produce its own hydrogen bonds, which can play a better role in modification and utilization. However, when the concentration of silver nitrate increases, the precipitation rate of silver accelerates, the interaction force between particles exceeds the steric resistance of polymer fibers, and the silver nanoparticles condense with each other. Therefore, it is difficult to control the morphology of silver particles. Once the size of the sample exceeds the nanometer level and becomes a micron level particle, it will lose the role of silver nanoparticles. We also deposited silver on unoxidized cellulose [46] (Fig. 3e–i). In Fig. 3f, we can see that NC and AgNPs are uniformly dispersed and white dots indicate the presence of NC in the main polymeric film. When NC is increased, and the white particles also increase gradually. Figure 3g is a cross section of silver particles on unoxidized nanocellulose, We can see that there are silver nanoparticles between each layer of the cellulose, which also proves that the silver nanoparticles are evenly distributed inside the cellulose, not just on the surface.

3.4 SEM–EDS Analysis

Figure 4 shows SEM–EDS spectra of pure PVA film and silver-loaded PVA composite film, the elements before and after the silver loading were shown in Table 1. It was found

Table 1 Surface elemental analysis data from EDS

Elements	Before silver loading		After silver loading	
	Weight percentage	Atom percentage	Weight percentage	Atom percentage
C	61.85	68.35	57.94	65.70
O	38.15	31.65	39.99	34.04
Ag	0	0	2.07	0.26

in Fig. 4a, SEM–EDS spectrum shows that there was a characteristic energy peak near 0.2–0.4 keV, which was characteristic of C and O. In Fig. 4b, except for the characteristic energy peak near 0.2–0.4 keV, strong energy characteristic peak also appeared at 3 keV, it turns out that both the atomic percentage and the weight percentage were small, this corresponds to the size of the nanosilver in Fig. 5. It also confirmed the presence of the element silver [47]. Also, the SEM–EDS spectrum of the materials was found to be C, O and Ag. They were 57.94%, 39.99% and 2.07% respectively.

3.5 TEM Analysis

Figure 5 is the TEM image of Ag-NC-PVA composite film. As can be seen from Fig. 5, most of the silver nanoparticles are wrapped in the nanocellulose, while only a small part is free outside the nanocellulose. This is due to the presence of a large number of carboxyl groups in the nanocellulose oxidized by TEMPO. In polymer systems, the charge

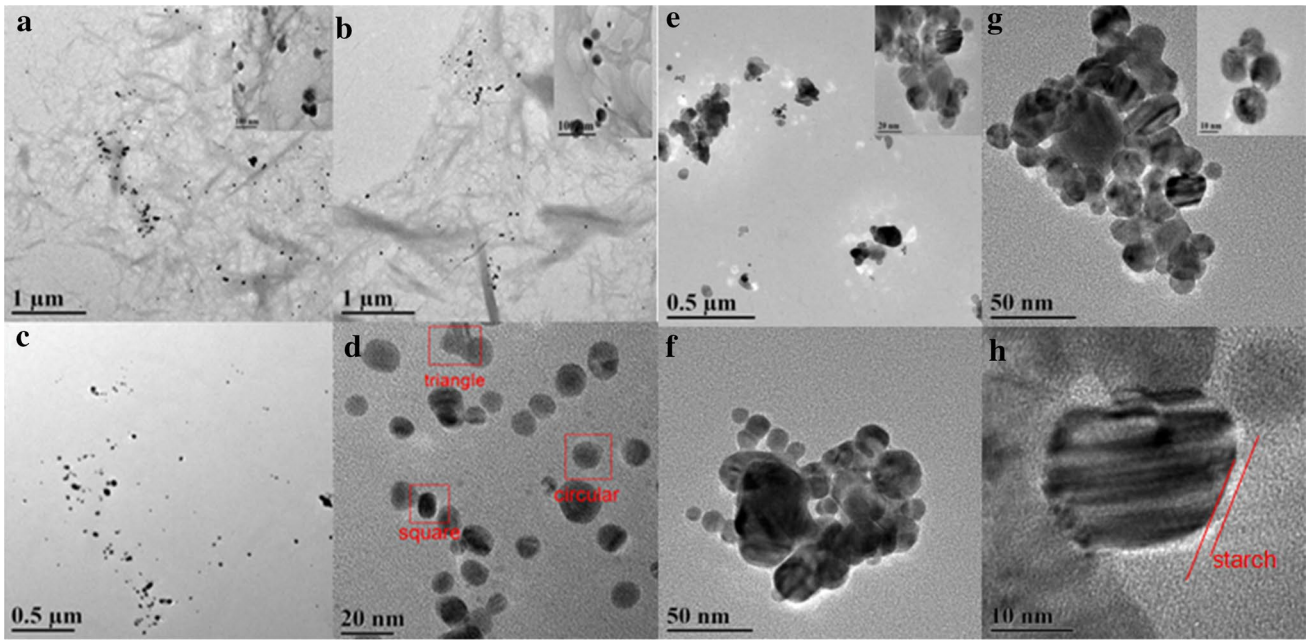

Fig. 5 TEM of nanocellulose polyvinyl alcohol membrane

attraction between the carboxyl group and Ag^+ creates a binding force that stabilises the free Ag^+ in the solution. After adding $NaBH_4$, Ag^+ is wrapped in it and reduced to nanosilver particles. As can be seen from Fig. 5c and d, the nanometer silver particles are visible, evenly dispersed and without obvious condensation. Nanosilver [48] is spherical, square or triangular in size, ranging in diameter from 5 to 20 nm. We also deposited silver on unoxidized cellulose (Fig. 5e–h). We can clearly see the prepared nanocomposite films, as can be seen from Fig. 5e and f, the size of silver nanoparticles was 10 to 15 nm. A small fraction of the cellulose is agglomerated, it causes the silver nanoparticles to fall off. In Fig. 6h, we can see that the structure of the starch is vesicular, and the internal structure of the vesicle is black compared with the edge. It shows that silver nanoparticles are successfully encapsulated in starch.

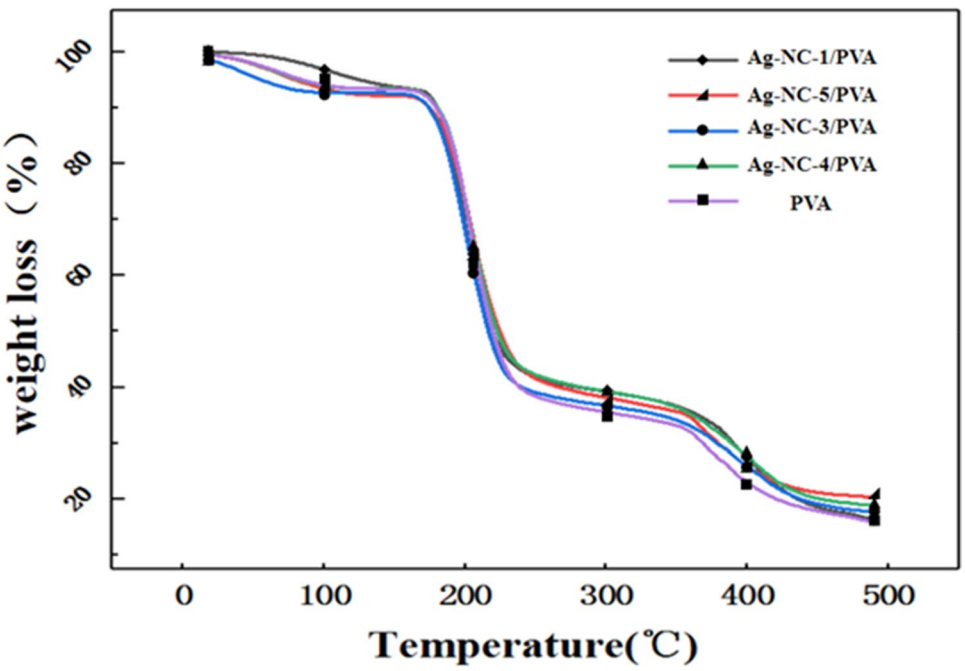

Fig. 6 TG analysis of PVA and Ag-NC-PVA

3.6 TG Analysis

Thermo gravimetric analysis (TG) for different sample films (Fig. 6). Approximately 12 mg samples were poured into the alumina crucible; the nitrogen stream was heated from 25 °C to 500 °C at 10 °C/min. For each degradation step in the composite films [49, 50], make measurements in duplicate. As shown in Fig. 6, All the samples showed an initial weight loss in the region 25 to 150 °C which can be ascribed to the evaporation loss of free water and combined water in the composite membrane surface. The weight loss in this range was around 15%. The second stage, PVA film and Ag-NC-PVA composite films have an obvious decline process between 150 °C and 500 °C, its weight loss exceeds 75%, thermal degradation of organic matter (NC, PVA) occurred in the composite films. When the temperature reaches 500 °C, the mass fraction no longer drops. At this time, the residue shall be carbonised residue and inorganic Ag, it was found that the residual of Ag-NC-PVA series in the composite film was larger than that of PVA; the Ag-NC had been successfully loaded on the PVA. However, the addition of Ag-NC did not significantly improve the thermal properties of the composite films. It was possible that the hydroxyl in Ag-NC molecule binds to the hydroxyl in PVA. As a result, the fiber structure in the matrix decreased, but the thermal stability of the composite membrane was not affected.

3.7 Water Uptake Analysis

Figure 7 shows water uptake of PVA and Ag-NC-PVA (sample 1: Ag-NC-1PVA; sample 2: Ag-NC-3PVA; sample 3: Ag-NC-4PVA; sample 4: Ag-NC-5PVA; sample 5: PVA). Water uptake of Ag-NC-PVA composite film and pure PVA film was tested. Different composite film was cut into different thin slices of equal size, and weigh them [51], then soak in water at room temperature for 24 h, weigh them one by one. Specific calculation formula:

$$\text{Water uptake } (\%) = \frac{M0 - M1}{M0} \times 100\%$$

M0: Weight after Water uptake; M1: Weight before Water uptake.

Found by test, the Water uptake of pure PVA film [52] was 59.1%, the Water uptake of Ag-NC-PVA composite film decreased, when the maximum concentration of silver ion was Ag-NC-5PVA, composite film Water uptake was the lowest, the size of 23.6%. Ag-NC-5PVA compared with pure PVA film, it decreased by 25.5%. It may be due to the presence of Ag nanoparticles and nanocellulose in PVA matrix, the original film dense structure was destroyed, or the hydroxyl groups of both bind to each other to form new through-holes in the film, the water-resistance of PVA composite film was improved.

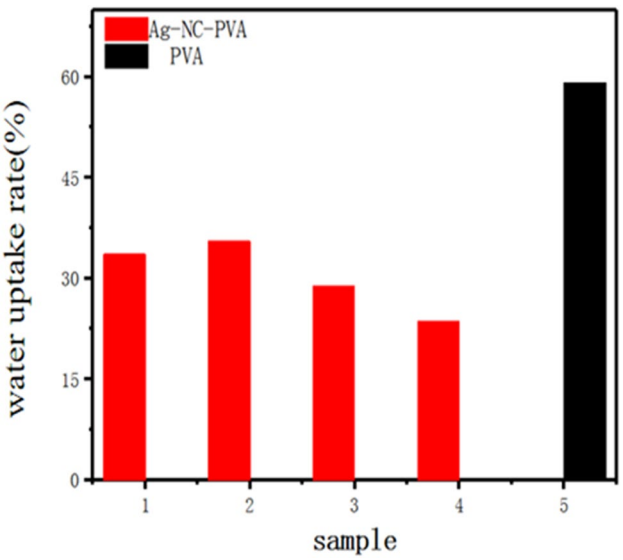

Fig. 7 Water uptake rate of PVA and Ag-NC-PVA

3.8 Mechanical Property Analysis

Figure 8a shows the tensile strength of PVA, Ag-NC and Ag-NC-PVA; Fig. 8b shows elongation at break of PVA, Ag-NC and Ag-NC-PVA (The weight of silver carried from left to right was 1%, 3%, 4%, 5% and 0%). The mechanical properties of Ag-NC, Ag-NC-PVA and pure PVA films were tested [53, 54], the elongation and tensile strength at break were evaluated, initial clamping distance of the tensile testing machine was set as 50 mm, drawing speed was set to 20 mm/min, a strip film sample (1.5 cm–7 cm) was placed into the sample for tensile strength and elongation at break test. The tensile strength and elongation at break of pure PVA film were 60.0 Mpa and 5.80% respectively, the tensile strength of PVA composite films after silver loading was higher than that before. The tensile strength of Ag-NC-4PVA was 71.3 MPa; tensile strength increased most obviously. It indicates the interaction between Ag, NC and PVA and leads to hydrogen bonding, the tensile strength of the composite film increases. In the process of stretching, cracks develop in the matrix and fiber is encountered. Interfacial debonding, fracture of the matrix and fiber, fiber pulling and other processes may occur, thus absorbing a lot of energy. Moreover, the development of cracks may not be in a plane, but may occur along different planes in the material, until the cracks through a plane of material is destroyed. The fracture energy of composite film was much higher than that of each component material, which shows the synergistic effect of composite material.

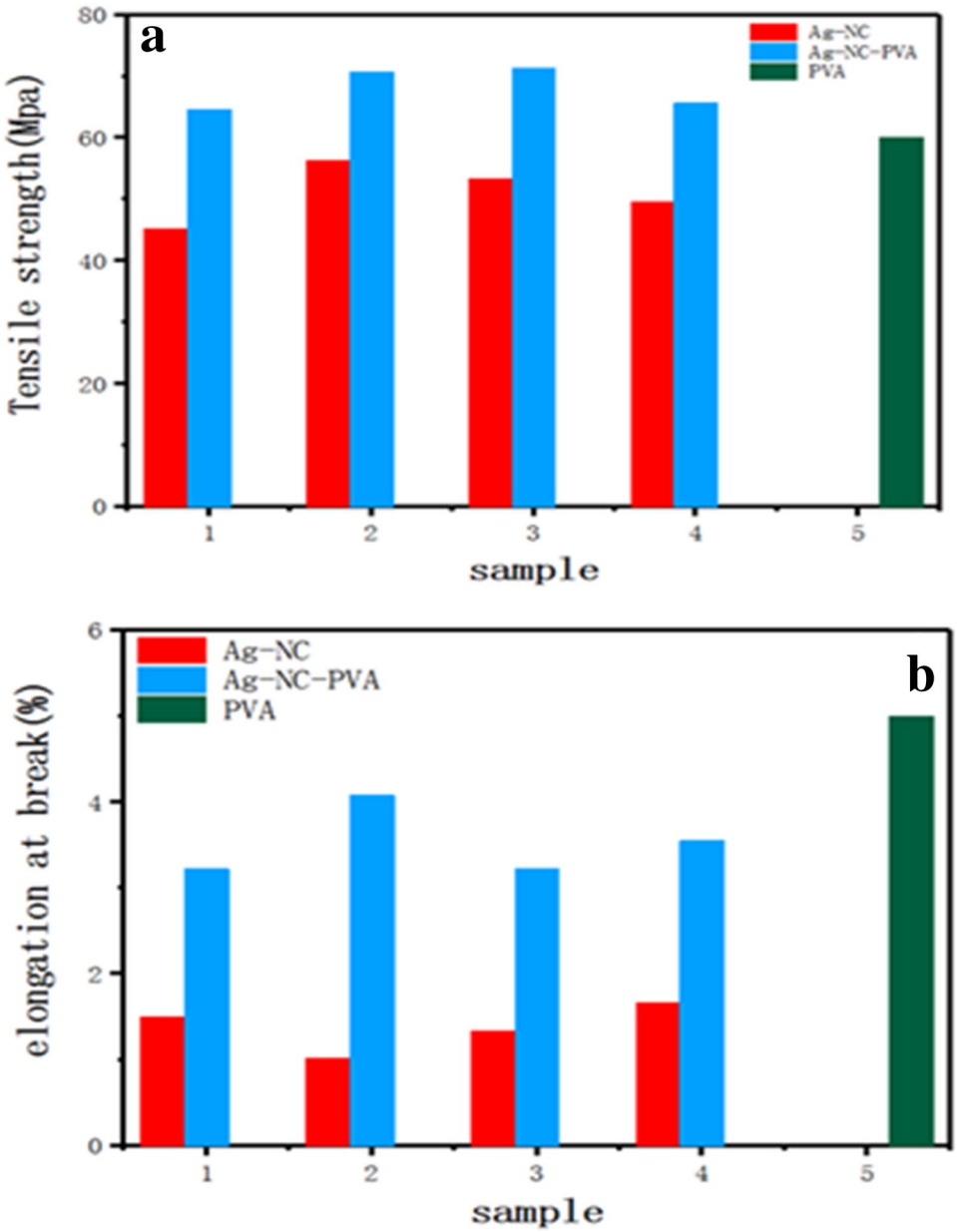

Fig. 8 **a** Shows tensile strength of PVA, Ag-NC and Ag-NC-PVA; **b** shows elongation at break of PVA, Ag-NC and Ag-NC-PVA

3.9 Antimicrobial Activity

To check for antimicrobial activity of the samples, weigh the film samples containing 1%, 3%, 4% and 5% Ag-NC-PVA equally. First prepare liquid medium and solid plate medium, *E. coli* was inoculated from inclined seeds into the seed medium, the seed liquid was cultured in a 37℃ constant temperature incubator for 12 h. Transfer 0.1 g seed liquid to solid plate medium and spread evenly. The prepared different silver-loaded Ag-NC-PVA film was placed in the centre of the medium. The size of a bacteriostasis zone was observed after 24 h constant temperature culture in 37 ℃ incubator. Because the material has the antibacterial ability, bacteria around the sample will produce a clear bacterial retarding ring: a bacteriostatic ring. Bacteria can grow rapidly in a solid medium.

Pure PVA film and Ag-NC-PVA films were set as the control group. The difference between a bacteriostatic zone and Ag-NC-PVA film radius was measured; each sample shall be measured at least three places (Fig. 9). The period of antibacterial effect is shown in Table 2. The antibacterial properties of the samples were evaluated by the width of antibacterial zone. When the bacteriostatic circle was larger, the bacteriostatic effect also increased. On the contrary, it indicates that the antibacterial effect of the material is worse.

We found that all the silver-bearing films except pure PVA film had a certain size of inhibition zone. When the silver content was 4%, at this time, the inhibition zone was the

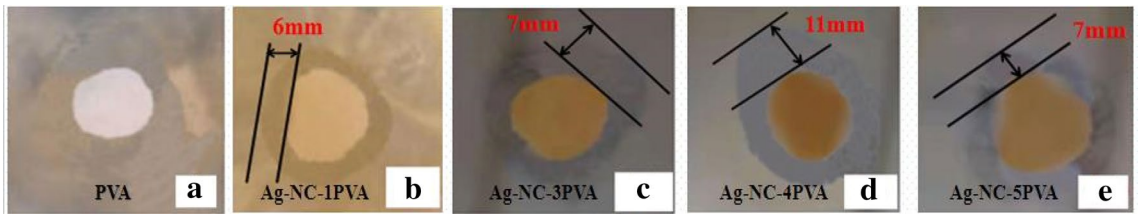

Fig. 9 Antibacterial activity of *E. coli* composite film samples

Table 2 Measure to bacterial inhibition of as-prepared samples

Time (days)	PVA	Ag-NC-1PVA	Ag-NC-3PVA	Ag-NC-4PVA	Ag-NC-5PVA
1	+	+	+	+	+
2	+	+	−	−	−
3	+	−	−	−	−
4	+	−	−	−	−
5	+	−	−	−	−
6	+	−	−	−	−
7	+	+	+	−	+
8	+	+	+	+	+

+: with *E. coli* growth, -: without *E. coli* growth from antimicrobial activity

largest. However, when the amount of silver was increased to a concentration of 5%, the concentration of inhibition zone began to decrease again; it shows that one of the main factors affecting the antibacterial effect of nanosilver is the dispersion degree of nanosilver. When nanosilver dispersion was better, the antibacterial effect of the composite was more obvious (Fig. 10).

4 Conclusions

(1) Ag-NC composite materials were prepared and uniformly dispersed in the PVA matrix.
(2) When the addition content of Ag-NC is 4%, the tensile strength is 71.3 MPa, which is nearly 15% higher than that of PVA.
(3) Most of the nanosilver particles have a smaller particle size, a size of 5 nm to 20 nm, and an average particle diameter of 10 nm.
(4) After antibacterial analysis, Ag-NC imparts excellent antibacterial properties to PVA. When the silver content is 4%, the inhibition effect is most obvious.

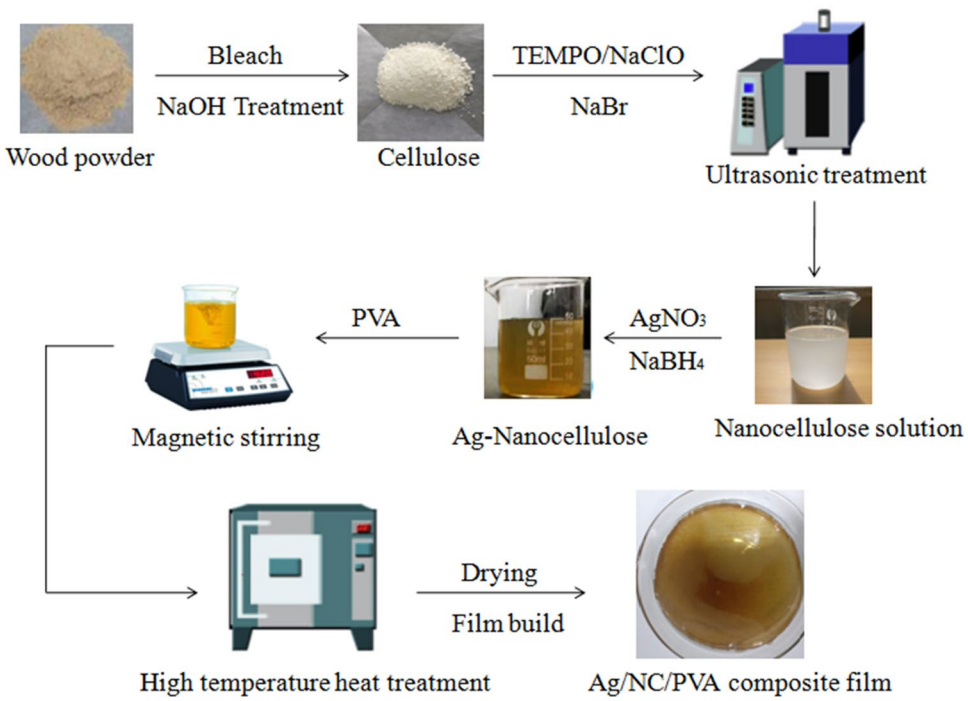

Fig. 10 The flow chart of preparation process of Ag/NC/PVA composite film

Funding This work was supported by Science and Technology Innovation Leading Project of Mongolia Autonomous Region (KCBJ2018013) and The Team of Inner Mongolia Autonomous Region Grassland Domain Innovation (2016).

Compliance with ethical standards

Conflict of interest No potential conflict of interest was reported by the authors.

References

1. V. Rajendran, B. Deepa, Studies on the structural, morphological, optical, electro-chemical and antimicrobial activity of bare, Cu and Ag @ WO_3 nanoplates by hydrothermal method. J. Inorg. Organomet. **28**(4), 1574–1586 (2018)
2. X.Y. Zhao, G.H. Yan, Y. Sun, Preparation of ethyl cellulose composite film with down conversion luminescence properties by doping perovskite quantum dots. Chem. Sel. **4**(21), 6516–6523 (2019)
3. X.D. Wang, C.H. Yao, F. Wang, Cellulose-based nanomaterials for energy applications. Small **13**(42), 1702240 (2017)
4. V. Siahpoush, S. Ahmadi-kandjani, A. Nikniazi, Effect of plasmonic coupling on photo thermal behavior of random nanoparticles. Opt. Commun. **420**, 52–58 (2018)
5. S. Ghiassi, M. Mokhtary, S. Sedaghat, H. Kefayati, Preparation, and antibacterial activity of chloroacetic acid immobilized on chitosan coated iron oxide decorated silver nanoparticles as an efficient catalyst for the synthesis of hexahydroquinoline-3-carboxamides. J. Inorg. Organomet. **29**(6), 1972–1982 (2019)
6. X.Y. Dong, L.X. Gao, W.Q. Zhang, Evolution of cobalt catalysis for catalytic construction of Si-H containing semi-penetrating networks: updated application in nanosilver-catalyzed alkynylation of paraformaldehyde. Chem. Sel. **1**(13), 4034–4043 (2016)
7. X.Y. Dong, Z.W. Gao, K.F. Yang, Nanosilver as a new generation of silver catalysts in organic transformations for efficient synthesis of fine chemicals. Catal. Sci. Technol. **5**(5), 2554–2574 (2015)
8. H. Tang, R. Wang, C.X. Zhao, Oxamide-modified g-C3N4 nanostructures: tailoring surface topography for high-performance visible light photocatalysis. Chem. Eng. J. **374**, 1064–1075 (2019)
9. Z. Ahmadi, M. Ashjari, R. Hosseini, Synthesis and morphological study of nanoparticles Ag/TiO2 ceramic and bactericidal investigation of polypropylene-Ag/TiO2 composite. J. Inorg. Organomet. **19**(3), 322–327 (2009)
10. V. Suba, G. Rathika, E. Ranjith Kumar, M. Saravanabhavan, Enhanced adsorption and antimicrobial activity of fabricated apocynaceae leaf waste activated carbon by cobalt ferrite nanoparticles for textile effluent treatment. J. Inorg. Organomet. **29**(2), 550–563 (2019)
11. G.V. Kumari, T. Mathavan, R. Srinivasan, The influence of physical properties on the antibacterial activity of lysine conjugated chitosan functionalized silver nanoparticles. J. Inorg. Organomet. **28**(6), 2418–2426 (2018)
12. Y. Haldorai, J.J. Shim, Chitosan-zinc oxide hybrid composite for enhanced dye degradation and antibacterial activity. Compos. Interfaces **20**(5), 365–377 (2013)
13. J. Koeser, M. Engelke, M. Hoppe, Predictability of silver nanoparticle speciation and toxicity in ecotoxicological media. Environ. Sci. Nano. **4**(7), 1470–1483 (2017)
14. L. Klapiszewski, T. Rzemieniecki, M. Krawczyk, Kraft lignin/silica-AgNPs as a functional material with antibacterial activity. Colloid Surf. B **134**, 220–228 (2015)
15. M.E. Barbinta-Patrascu, C. Ungureanu, S.M. Iordache, Eco-designed biohybrids based on liposomes, mint-nanosilver and carbon nanotubes for antioxidant and antimicrobial coating. Mater. Sci. Eng. C **39**, 177–185 (2014)
16. S.M. Xu, W.J. Yu, X.L. Yao, Nanocellulose-assisted dispersion of graphene to fabricate poly(vinyl alcohol)/graphene nanocomposite for humidity sensing. Compos Sci Technol. **131**, 67–76 (2016)
17. G.A. Sotiriou, S.E. Pratsinis, Engineering nanosilver as an antibacterial, biosensor and bioimaging material. Curr Opin Chem Eng. **1**(1), 3–10 (2011)
18. S.Y. Zhang, X.Y. Xu, T.S. Lin, Recent advances in nano-materials for packaging of electronic devices. J Mater Sci-Mater Electron. **30**(15), 13855–13868 (2019)
19. B.B. Liu, A.R. Chen, R.F. Wang, T. Sun, Sputtered Ge/Si nanocomposite films as high performance anode materials for lithium-ion battery. J. Inorg. Organomet. **30**(2), 427–437 (2020)
20. Y.L. Cui, Z. Sun, Q.C. Zhuang, Electrochemical properties of a 4.7 V-Class $LiNi0.5Mn1.5O_4$ positive electrode material for high power Li-Ion battery. J. Inorg. Organomet. **21**(4), 893–899 (2011)
21. D. Sharma, N. Jaggi, Two-gap superconductivity in niobium carbide-coated single-walled carbon nanotubes: a first-principles study. J. Supercond. Nov. Magn. **30**(2), 371–377 (2017)
22. S. Niakan, M. Niakan, S. Hesaraki, M.R. Nejadmoghaddam, Comparison of the antibacterial effects of nanosilver with 18 antibiotics on multidrug resistance clinical isolates of acinetobacter baumannii. Jundishapur J. Microb. **6**, 5 (2013)
23. K. Madhumathi, S. Abhilash, Development of novel chitin/nanosilver composite scaffolds for wound dressing applications. J. Mater. Sci. Mater. Electron. **21**(2), 807–813 (2010)
24. Y.A. Kahnouji, E. Mosaddegh, M.A. Bolorizadeh, Detailed analysis of size-separation of silver nanoparticles by density gradient centrifugation method. Mater. Sci. Eng. C. **103**, 109817 (2019)
25. S.S. Irhayyim, S.R. Ahmed, A.A. Annaz, Mechanical performance of micro-Cu and nano-Ag reinforced Al-CNT composite prepared by powder metallurgy technique. Mater. Res. Express. **6**(10), 105071 (2019)
26. S.M. Amini, Preparation of antimicrobial metallic nanoparticles with bioactive compounds. Mater. Sci. Eng. C **103**, 109809 (2019)
27. P.P. Kumar, R.L. Kalyani, S.C. Veerla, Biogenic synthesis of stable silver nanoparticles via *Asparagus racemosus* root extract and their antibacterial efficacy towards human and fish bacterial pathogens. Mater. Res. Express. **6**(10), 104008 (2019)
28. L.M. Mahlaule-Glory, Z. Mbita, M.M. Mathipa, Biological therapeutics of AgO nanoparticles against pathogenic bacteria and A549 lung cancer cells. Mater. Res. Express. **6**(10), 105402 (2019)
29. H.M. Abd El Salam, H.N. Nassar, T. Zaki, Antimicrobial activities of green synthesized Ag nanoparticles @ Ni-MOF nanosheets. J. Inorg. Organomet. **28**(6), 2791–2798 (2018)
30. M. Alqahtany, P. Khadka, I. Niyonshuti, Nanoscale reorganizations of histone-like nu-cleoid structuring proteins in *Escherichia coli* are caused by silver nanoparticles. Nanotechnology **30**(38), 385101 (2019)
31. L. Baldino, J. Aragon, G. Mendoza, Production characterization and testing of antibacterial PVA membranes loaded with HA-Ag3PO4 nanoparticles produced by SC-CO2 phase inversion. J Chem Technol Biot. **94**(1), 98–108 (2019)
32. H.Y. Li, H.Y. Jing, Y.D. Han, Interfacial evolution behavior of AgSbTe2.01/nanosil-ver/Cu thermoelectric joints. Mater. Des. **89**, 604–610 (2016)
33. Q.Y. Xu, Y.H. Mei, X. Li, Correlation between interfacial microstructure and bonding strength of sintered nanosilver on ENIG and electroplated Ni/Au direct-bond-copper (DBC) substrates. J. Alloy Compd. **675**, 317–324 (2016)

34. J.T. Sun, C.C. Wang, H.T. Lee, Preparation and characterization of polysulfone/Na-nosilver-doped activated carbon nanocomposite. Polym. Sci. A. **60**(1), 90–101 (2018)
35. L. Jiang, G.Y. Lei Thomas, D.T. Ngo Khai, Evaluation of thermal cycling reliability of sintered nanosilver versus soldered joints by curvature measurement. IEEE Trans. Compon Pack Manuf. Technol. **4**(5), 751–761 (2014)
36. Y.H. Mei, G. Chen, X. Li, Evolution of curvature under thermal cycling in sandwich assembly bonded by sintered nanosilver paste. Solder Surf. Mt. Technol. **25**(2), 107–116 (2013)
37. F. Zandpour, A.R. Allafchian, M.R. Vahabi, Green synthesis of silver nanoparticles with the Arial part of *Dorema ammoniacum* D. extract by antimicrobial analysis. IET Nanobiotechnol. **12**(4), 491–495 (2018)
38. A. Laik, A.A. Shirzadi, G. Sharma, Microstructure and interfacial reactions during vacuum brazing of stainless steel to titanium using Ag-28 pct Cu alloy. Metall. Mater. Trans. A. **46A**(2), 771–782 (2015)
39. O. Crisan, A.D. Crisan, M. Enculescu, Interfacial mechanisms of novel laser-irradiated L1(0)-based nanocomposite magnets. Appl Phys A. **122**(4), 411 (2016)
40. N. Maity, A. Mandal, A.K. Nandi, Synergistic interfacial effect of polymer stabilized graphene via non-covalent functionalization in poly(vinylidene fluoride) matrix yielding superior mechanical and electronic properties. Polymer **88**, 79–93 (2016)
41. M.S. Islam, N. Akter, M.M. Rahman, Mussel-inspired immobilization of silver nanoparticles toward antimicrobial cellulose paper. ACS Sustain. Chem. Eng. **6**(7), 9178–9188 (2018)
42. O.B. Ceran, B. Simsek, S. Doruk, Effects of dispersed and powdered silver nanoparticles on the mechanical, thermal, electrical and durability properties of cementitious composites. Constr. Build Mater. **222**, 152–167 (2019)
43. H. Celebi, M. Gurbuz, A.S. Koparal, A. Dogan, Development of antibacterial electro spun chitosan/poly(vinyl alcohol) nanofibers containing silver ion-incorporated HAP nanoparticles. Compos. Interfaces. **20**(9), 799–812 (2013)
44. S. Wang, S.Y. Niu, H.S. Li, Synthesis and controlled morphology of Ni@Ag core shell nanowires with excellent catalytic efficiency and recyclability. Nanotechnology **30**(38), 385603 (2019)
45. S. Addanki, J. Jayachandiran, K. Pandian, Development of optical sensors for the quantitative detection of ozone using gold and silver thin film nanoislands. Sens Actuator B-Chem. **210**, 17–27 (2015)
46. M.S. Sarwar, M. Niazi, Z. Jahan, T. Ahmad, Preparation and characterization of PV-A/nanocellulose/Ag nanocomposite films for antimicrobial food packaging. Carbohydr. Polym. **184**, 453–464 (2018)
47. G.H. Qin, J. Liu, Y. Xue, Enhanced stability of antimicrobial bamboo fiber by launching ultra fine silver particles in a sodium dodecyl sulfate micro emulsion system. Text Res J. **87**(20), 2505–2512 (2017)
48. S. Anjum, A. Sharma, M. Tummalapalli, A novel route for the preparation of silve-r loaded polyvinyl alcohol nanogels for wound care systems. Int. J. Polym. Mater. **64**(17), 894–905 (2015)
49. A. Chaturvedi, A.K. Bajpai, J. Bajpai, Evaluation of poly (vinyl alcohol) based cryogel-zinc oxide nanocomposites for possible applications as wound dressing materials. Mater. Sci. Eng. C **65**, 408–418 (2016)
50. J.H. Lin, Z.I. Lin, Y.J. Pan, Thermoplastic polyvinyl alcohol/multiwalled carbon nanotube composites: Preparation, mechanical properties, thermal properties, and electromagnetic shielding effectiveness. J. Appl. Polym. Sci. **133**(21), 43474 (2016)
51. Z.W. Abdullah, Y. Dong, Biodegradable and water resistant poly (vinyl) alcohol (PVA)/starch (ST)/glycerol (GL)/halloysite nanotube (HNT) nanocomposite films for sustainable food packaging. Front Mater. **6**, 34 (2019)
52. W. Tanan, J. Panichpakdee, S. Saengsuwan, Novel biodegradable hydrogel based on natural polymers: synthesis, characterization, swelling/reswelling and biodegradability. Eur Polym J. **112**, 678–687 (2019)
53. A. Gautam, P. Komal, Synthesis of montmorillonite clay/poly (vinyl alcohol) nanocomposites and their mechanical properties. J. Nanosci. Nanotechnol. **19**(12), 8071–8077 (2019)
54. F. Wahid, F.P. Wang, Y.Y. Xie, Reusable ternary PVA films containing bacterial cellulose fibers and epsilon-polylysine with improved mechanical and antibacterial properties. Colloid Surf. B. **183**, 110486 (2019)